Chemical Science

ROYAL SOCIETY OF CHEMISTRY

EDGE ARTICLE

View Article Online
View Journal | View Issue

Cite this: *Chem. Sci.*, 2024, **15**, 15907

All publication charges for this article have been paid for by the Royal Society of Chemistry

Received 24th June 2024
Accepted 28th August 2024

DOI: 10.1039/d4sc04165h

rsc.li/chemical-science

Ultralow thermal conductivity and thermally-deactivated electrical transport in a 1D silver array with alternating δ-bonds†

Nahid Hassan, [a] Suneetha Nagaraja,[b] Sauvik Saha, [a] Kartick Tarafder [b] and Nirmalya Ballav *[a]

We report the synthesis of a (TMA)$AgBr_2$ (TMA = tetramethylammonium) crystal, which comprises inorganic anionic chains of $-(AgBr_2)_\infty-$ stabilized by columnar stacks of organic TMA cations with a periodic arrangement of shorter and longer Ag(I)···Ag(I) bonds, even though all the Ag(I) ions are chemically equivalent. The presence of two chemically non-equivalent bridging Br ions is attributed to the primary cause of such an unusual arrangement, as clearly visualized in the charge density plot of (TMA)$AgBr_2$ extracted from the theoretical calculations based on density functional theory. Remarkably, we identified from the orbital-projected density of states the existence of alternate δ-like bonding involving d_{xy} orbitals of $4d^{10}$ Ag(I), which was attributed to the cause for ultralow thermal conductivity and thermally-deactivated electrical transport in (TMA)$AgBr_2$. Barring the energetics, our observations on the existence of a δ-bond will shed new light in understanding the nature of metal–metal chemical bonding and its unprecedented implications.

Introduction

Metallophilic interactions are a unique variant of weak attractive forces in chemical bonding, acting between atoms with interatomic distance less than the sum of their van der Waals radii. These interactions lead to novel physicochemical properties in the systems. Typically, metal ions with closed-shell (d^{10} and s^2) or pseudo-closed shell (d^8) electronic configurations are known to exhibit metallophilic interactions.[1–7] Owing to their unusual nature, which is distinct from the conventional concepts of chemical bonding, the past few decades have seen a growing interest in generating and understanding such metallophilic interactions, especially involving univalent coinage metal (Au(I), Ag(I) and Cu(I)) compounds.[8–15] Initially, significant research focused on exploring aurophilic (Au(I)···Au(I)) interactions, followed by argentophilic (Ag(I)···Ag(I)) interactions and cuprophilic (Cu(I)···Cu(I)) interactions. Argentophilicity is known to impart various interesting properties in systems and has applications such as dynamic chirality inversion in metal organic supramolecular polymers, circularly polarized luminescence in alkynyl-stabilized clusters, capturing and photocatalysis of mustard-gas simulant in a porphyrinic cluster, chemical fixation of carbon dioxide in a two-dimensional metal–organic framework, combating antibiotic resistance against *Staphylococcus aureus*, as bioprotective materials for combating superbacteria, and artificial light-harvesting.[16–22] However, argentophilic interactions have so far been observed in discrete complexes, clusters, and supramolecular assemblies, except a report on an uninterrupted one-dimensional silver array stabilized by specific interactions with the base pairs of DNA.[23] The implications arising from the long-range ordering of such weak forces of attraction can be intriguing; for example, the silver–DNA hybrid nanowire is expected to facilitate electrical conduction, similar to earlier observations of the metallophilic interactions in linear-chains imparting electrical conductivity. Notably, all these materials can be considered as semiconductors *viz.* they exhibit the thermally-activated electrical transport property. The question is: what would happen if the long-range metallophilic interactions are periodically interrupted? Herein, we synthesized an organic-inorganic hybrid crystal, (TMA)$AgBr_2$, (TMA = tetramethylammonium cation), exhibiting a one-dimensional array of Ag(I) ions bridged with Br ions, and we identified an alternating arrangement of the argentophilic interactions, which is unprecedented.

Results

Single crystals of (TMA)$AgBr_2$ were synthesized following a controlled cooling crystallization process. The crystal structure was obtained by a single-crystal X-ray diffraction (SCXRD)

[a]*Department of Chemistry, Indian Institute of Science Education and Research, Dr. Homi Bhabha Road, Pune – 411 008, India. E-mail: nballav@iiserpune.ac.in*

[b]*Department of Physics, National Institute of Technology Karnataka, Surathkal, Mangalore – 575 025, India*

† Electronic supplementary information (ESI) available. CCDC 2352448–2352450. For ESI and crystallographic data in CIF or other electronic format see DOI: https://doi.org/10.1039/d4sc04165h

technique using an orthorhombic crystal system with the space group *Immm*, having the unit cell parameters as follows: a = 6.7744(13) Å, b = 9.1274(19) Å, c = 15.003(3) Å, V = 927.675 Å^3 (Tables S1–S3†). The crystal is made up of polymeric –$(AgBr_2)_n$– anionic chains stabilized by stacked TMA cations (Fig. 1a and S1a–c†). The –$(AgBr_2)_n$– chains are isolated from each other, and a single chain is surrounded by six stacks of TMA cations. The Ag(I) ions in the chains are tetrahedrally coordinated to four Br^- ions, with each Br^- ion being connected to two neighboring Ag(I) cations (Fig. 1b and S2a–c†). Interestingly, every Ag(I) cation exhibits an additional Ag(I)···Ag(I) bond with one of its nearest neighbors, with a bond distance of 3.151 Å (well below the sum of their van der Waals radii) – indicating the presence of argentophilic interactions. In general, metallophilic interactions are considered to exist in a compound if the metal–metal separation is shorter than the sum of their van der Waals radii[10] and it is not related to Shannon ionic or crystal radii,[24] which are usually considered for metal–halide bonds. The Ag(I)···Ag(I) distance involving the opposite nearest neighbor is measured to be 3.623 Å and consequently, no bonding was observed (*viz.* argentophilic interactions are absent). Therefore, a one-dimensional silver array with alternating argentophilic interactions is clearly identified in (TMA)$AgBr_2$.

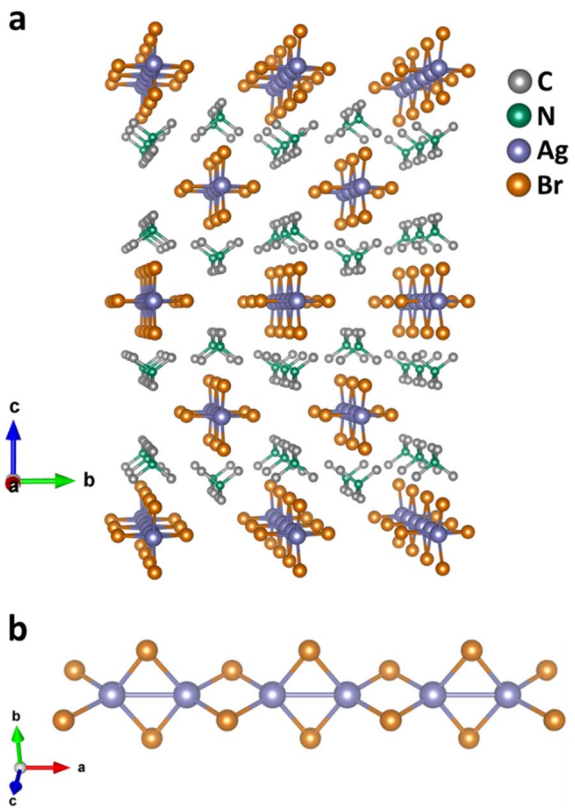

Fig. 1 Crystal structure of (TMA)$AgBr_2$. (a) Extended arrangements of TMA cations and $(AgBr_2)_n^{n-}$ anionic chains viewed along the crystallographic *a*-axis (perspective view, H atoms are omitted for clarity). All the $(AgBr_2)_n^{n-}$ polymeric chains are segregated from one another, and each chain is surrounded by six stacks of TMA cations running along the *a*-axis. (b) Zoomed-in view of a single inorganic $(AgBr_2)_n^{n-}$ chain along the crystallographic *a*-axis, showing the alternate Ag···Ag (argentophilic) interactions.

Such an alternating arrangement of Ag ions is completed with the presence of two Br^- ions, here assigned as Br1 and Br2. The Br1 ion is bridged to the Ag(I)···Ag(I) bonding pair with a distance of 2.692 Å and angle of 71.66°, while the Br2 ion is bridged to the Ag(I)···Ag(I) non-bonding pair with a distance of 2.738 Å and an angle of 82.86° (Fig. S2†). Another important consideration of the overall energetics that could influence the contribution of ionic interactions in the system is the closest distance between Br^- ions and the TMA cation: 5.039 Å for Br1 and 4.203 Å for Br2. The powder X-ray diffraction (PXRD) pattern matched very well with the simulated XRD pattern from SCXRD analysis, thereby confirming the phase-purity of our bulk sample (Fig. S3†). X-ray photoelectron spectroscopy (XPS) was employed to probe the oxidation state of Ag. The Ag 3d photoemission signal, with peaks for Ag $3d_{3/2}$ and Ag $3d_{5/2}$ (due to spin–orbit coupling) at respective binding energy values of 373.4 eV and 367.4 eV ensured the exclusive presence of Ag(I) in (TMA)$AgBr_2$ (Fig. S4†).[25,26] Thermogravimetric analysis (TGA) revealed no thermal degradation up to 600 K, attributed to the excellent tolerance of (TMA)$AgBr_2$ to thermal energy (Fig. S5†).

Electronic structure calculations on the (TMA)$AgBr_2$ system were performed using density functional theory (DFT). A direct band gap (E_g) of 3.53 eV with the valence band maxima (VBM) as well as the conduction band minima (CBM) located at the gamma (G) point was identified (Fig. S6†). This theoretically estimated band gap (E_g) is in reasonable agreement with the experimentally obtained value of 4.1 eV (Fig. S7†). The orbital projected density of states (DOS) plots suggest that the primary contributions towards VBM and CBM originate from the Ag4d–Br4p and Ag5s–Br4p orbitals, respectively (Fig. S8†). Notably, the organic part, TMA, has negligible contribution towards VBM and CBM, further implying the importance of the inorganic –$(AgBr_2)_n$– chain in predominantly shaping the electronic band structure. The partial charge density plots clearly depict periodic accumulation of electronic charge between the alternate Ag atoms, *viz.* a direct visualization of the alternate argentophilic interactions in the one-dimensional Ag chain (Fig. 2a). Critically looking at the orbital contributions in generating the $4d^{10}$···$4d^{10}$ Ag(I)···Ag(I) bond, as reflected in the orbital projected density of states, the overlap between the d_{xy} orbitals was predominantly identified to be the origin of the argentophilic interactions in (TMA)$AgBr_2$ – resembling a classical δ-like bonding scenario (Fig. 2b and c).[27–29] Earlier, in view of the energetics,[3] argentophilic interactions were primarily assigned to be weak non-covalent interactions, even weaker than ionic and dispersion interactions; however, our DFT calculations clearly reveal the involvement of δ-bonding in these argentophilic interactions. Being very much sensitive to distance, the presence or absence of δ-bonding can have a significant impact on the electronic structure,[28] rendering such systems to behave as topological materials.

The unique electronic and crystal structure of (TMA)$AgBr_2$ inspired us to measure its thermal transport properties. The variable temperature thermal diffusivity (α) as well as the specific heat capacity (C_p) for the (TMA)$AgBr_2$ system were

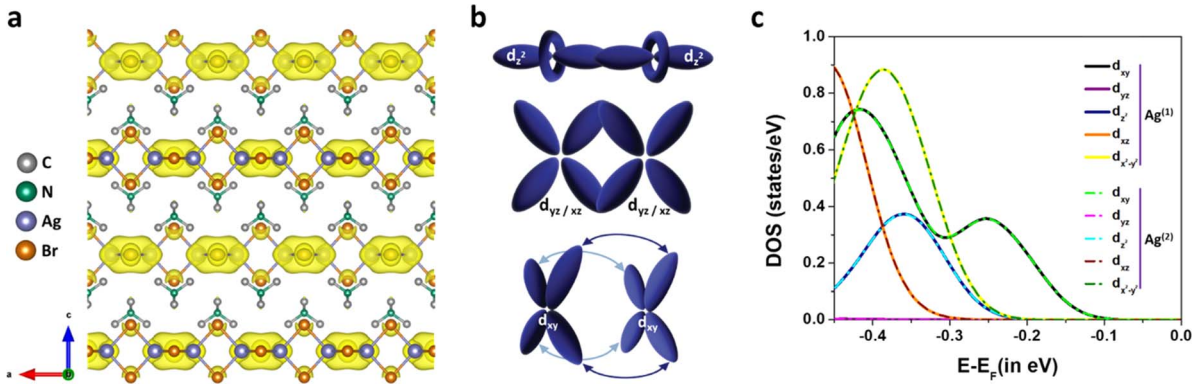

Fig. 2 Visualization of argentophilic interactions in (TMA)$AgBr_2$. (a) Charge density plot illustrating the distribution of electronic charge in the alternate Ag⋯Ag region depicting interrupted argentophilic interactions (electron accumulation is represented by yellow isosurfaces). (b) Possible orbital overlapping scenarios involved in the M⋯M σ-bond (top; $d_z^2 \cdots d_z^2$), π-bond (middle; $d_{yz/zx} \cdots d_{yz/zx}$) and δ-bond (bottom; $d_{xy} \cdots d_{xy}$). (c) Orbital-projected density of states (DOS) plots showing the orbital contributions in the Ag⋯Ag region.

collected in the temperature range ∼300 K to ∼380 K. The α was $\sim 1.83 \times 10^{-3}$ cm^2 s^{-1} at 307 K, which gradually decreased with increasing the temperature and reached a value of $\sim 1.57 \times 10^{-3}$ cm^2 s^{-1} at 375 K (Fig. 3a). C_p exhibited the opposite trend, with a lower value of ∼1.68 J g^{-1} K^{-1} at 300 K and a higher value of ∼2.05 J g^{-1} K^{-1} at 380 K (Fig. 3b). The thermal conductivity (κ) of the material was then calculated using the following equation: $\kappa = \alpha\rho C_p$, where ρ is the density.[30] Remarkably, an ultralow value of κ (∼0.6 W m^{-1} K^{-1}) was reproducibly achieved at near room-temperature for the (TMA)$AgBr_2$ system (Fig. 3c), resembling the benchmark values of all-inorganic halide perovskites $CsPbI_3$ (∼0.45 W m^{-1} K^{-1}), $CsPbBr_3$ (∼0.42 W m^{-1} K^{-1}) and $CsSnI_3$ (∼0.38 W m^{-1} K^{-1}).[31] An intrinsically low thermal conductivity in $CuBiI_4$ (∼0.34–0.28 W m^{-1} K^{-1}) was attributed to strong antibonding I(p)–Cu(d) states[32] and likewise the primary involvement of Br(p)–Ag(d) states in the formation of the valence band and conduction band of (TMA)$AgBr_2$. Further, bonding heterogeneity in $AgPbBiSe_3$ (ref. 33) leading to an ultralow thermal conductivity resembles an alternating arrangement of δ-bond facilitating ultralow thermal conductivity in (TMA)$AgBr_2$. Additionally, the organic cations could induce structural modulations, further lowering the thermal conductivity.[34]

The electrical transport properties of the (TMA)$AgBr_2$ system were also evaluated upon recording the temperature-dependent current–voltage (*I–V*) profiles on the pelletized sample using our two-probe configuration[13] (Fig. S9†). Upon gradually increasing the temperature from 298 K to 333 K, the current value gradually increased, which therefore contradicts the traditional conduction of electrons in semiconductors and suggests a thermally-deactivated electrical transport mechanism in the (TMA)$AgBr_2$ system, which is typically observed in metals, *viz.* metallic conduction (Fig. 4a).[35] The electrical conductance values were extracted from the *I–V* profiles, and the conductance value decreased from $\sim 8 \times 10^{-10}$ S at 298 K to $\sim 5 \times 10^{-13}$ S at 333 K (Fig. S10a†). Such a remarkable change in the electrical conductance value (by *ca.* 10^3 times) could be associated with a structural phase transition in the system, and in order to probe it, variable temperature SCXRD data and PXRD patterns were collected for the (TMA)$AgBr_2$ sample. Interestingly, the SCXRD data and the PXRD patterns did not show any appreciable change in the lattice parameters or crystal symmetry (Tables S4–S6† and Fig. 4b). This established the fact that the electrical transport behavior of (TMA)$AgBr_2$ is inherent in the solitary phase and that internal electronic and phononic changes might be responsible for the thermally-deactivated

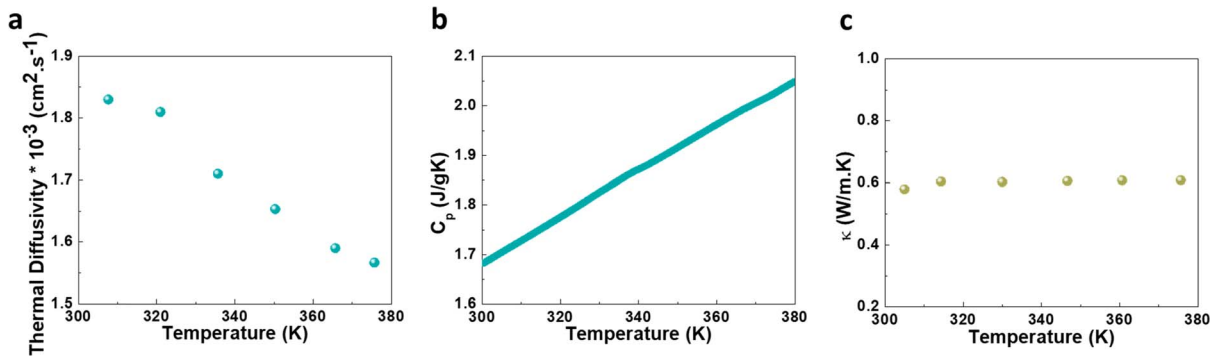

Fig. 3 Possibility of electron-phonon coupling. (a) Thermal diffusivity of (TMA)$AgBr_2$ as a function of temperature. (b) Heat capacity (C_p) of (TMA)$AgBr_2$ as a function of temperature. (c) Variable temperature thermal conductivity of (TMA)$AgBr_2$ yielding an ultra-low value.

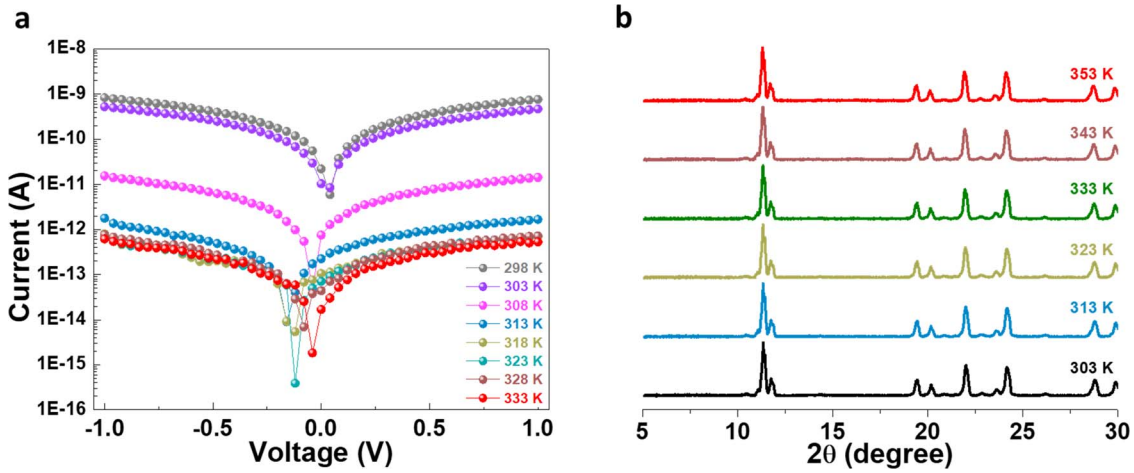

Fig. 4 Metallic conduction without structural change. (a) Variable-temperature current–voltage (I–V) diagram of (TMA)$AgBr_2$ in the temperature range from 298 K to 333 K, illustrating thermally deactivated charge transport. (b) Variable temperature PXRD patterns showing the retention of the structural phase over the temperature range.

charge transport phenomenon. I–V measurements were also carried out to estimate the room-temperature electrical conductivity of (TMA)$AgBr_2$, using a collinear four probe set-up, and the value was calculated to be $\sim 5.90 \times 10^{-6}$ S m^{-1} (Fig. S10b†).

Unlike normal semiconductors, upon light irradiation (450 nm) (possibly due to trapped and/or defect state mediated absorption within the band gap, *cf.* Fig. S7†), the electrical conductance value of (TMA)$AgBr_2$ dropped by more than an order of magnitude (Fig. 5) – a phenomenon known as negative photoconductivity (NPC). Various explanations have been reported for NPC; to mention a few: the generation of secondary hot electrons, formation of scattering centers, excitation into deep defect levels, surface plasmon resonance, charge carrier trapping due to moisture adsorption, trion formation, the presence of DX (D: donor atom, X: unspecified lattice defect) like centers, light-activated trap states, and thermal broadening of electron distribution.[36] Particularly, in halide perovskites and related systems, NPC was attributed to the creation of light-activated metastable trap states[37] and the self-trapping of charge carriers.[38] Similar mechanisms could also be responsible for the negative photoconductivity in our (TMA)$AgBr_2$ system. Notably, in our earlier-reported (TMA)Ag_2Br_3 system,[13] under identical conditions of light irradiation, the electrical conductivity value was observed to be unaltered, which clearly highlights the implications of a distinctive structure and chemical bonding scenarios, *viz.* the structure–property relationship.

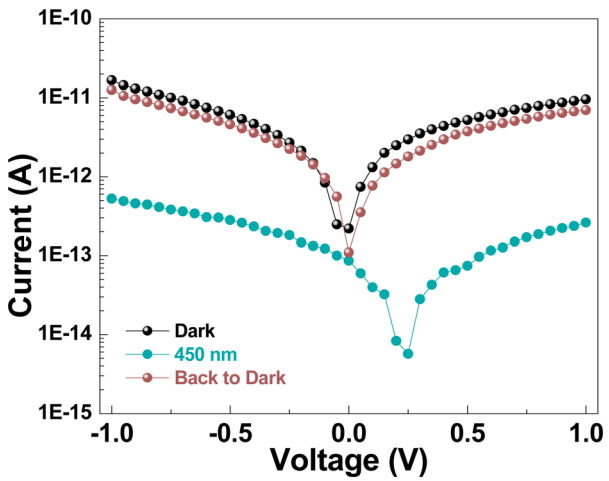

Fig. 5 Current–voltage (I–V) plots of (TMA)$AgBr_2$ in the dark and under the influence of 450 nm laser irradiation.

To further emphasize the importance of δ-bonding, *i.e.*, argentophilic interactions behind the metal-like electrical conduction in the (TMA)$AgBr_2$ system, we have collected variable temperature I–V profiles for commercially available AgBr using a conventional two-probe setup on a pelletized sample. The phase-purity of AgBr was confirmed by collecting the PXRD pattern, which matched well with the simulated pattern (ICSD 1627211), without the presence of any impurity peaks (Fig. S11†). Notably, in the cubic crystal structure of AgBr, the closest Ag···Ag distance is identified as 4.059 Å (Fig. S12a†), which is beyond the upper limit of argentophilic interactions. Upon increasing the temperature, the electrical conductance value of the AgBr sample gradually increased – a clear signature of the thermally-activated electrical transport typically valid for semiconductors (Fig. S12b†). The thermal conductivity value of AgBr was estimated to be ~ 1.34 W m^{-1} K^{-1} at near room-temperature (Fig. S13a–c†). Such a significantly higher κ value of AgBr highlights the influence of Ag···Ag interaction in imparting a comparatively lower thermal conductivity value for the (TMA)$AgBr_2$ system. Thermal conductivity values of relevant systems, starting from the conventional all inorganic and inorganic–organic halide perovskites to more recently reported diverse Cu(I) and Ag(I) based compounds, are summarized in Table S7.†

Raman spectra of the (TMA)$AgBr_2$ sample were recorded at 298 K and 353 K to investigate the possible origin of the ultralow thermal conductivity as well as the thermally-deactivated charge transport; the spectral features were almost unaltered, expect in

two regions: 1350–1450 cm^{-1} and 100–150 cm^{-1} (Fig. S14†). The Raman peaks at 1370 cm^{-1} and 1400 cm^{-1} (which can be denoted as the $\nu_2^{CH}(a_1)$-CH_3 symmetric deformation in the organic part of (TMA)$AgBr_2$)[39] were respectively blue-shifted to 1381 cm^{-1} and 1411 cm^{-1} upon increasing the temperature, demonstrating an alteration in the specific phonon mode as a function of temperature (Fig. S15b†). For the Raman peak at 130 cm^{-1}, upon elevating the temperature, there is a significant enhancement in the intensity (almost twice compared to that between the normalized spectra with respect to the highest intensity peak at 3020 cm^{-1}); this peak can be a characteristic of the Ag(I)···Ag(I) bond (Fig. S15a†). Typically, Raman intensity is directly related to the polarizability (and symmetry); so as to say, a higher spectral intensity reflects an increase in the bonding covalence of the system. Therefore, on the one hand, there is a possibility of an exotic electron-phonon coupling; on the other hand, upon increasing the temperature, an extended electron delocalization along the Ag chain is anticipated, which altogether led to the unusual metallic conduction in the (TMA)$AgBr_2$ system.

Conclusions

Looking at the trends of both electrical conductance (and so the electrical conductivity) and thermal conductivity values of (TMA)$AgBr_2$, the ratio of the thermal conductivity (κ) to the electrical conductivity (σ) would increase with increasing temperature. Such an important observation apparently validates the applicability of the Wiedemann–Franz law ($\kappa/\sigma \propto T$) to our (TMA)$AgBr_2$ system, *viz.* metal-like conduction; key to this observation was the presence of alternating argentophilic interactions in a one-dimensional array of the Ag(I) ions, which is unprecedented. Our study highlighting the concept of δ-bonding within metallophilic interactions will stimulate experimental as well as theoretical investigations on the electron–phonon coupling in such unique Ag-based systems; further, it may open the door for development of organic–inorganic hybrid materials with ultra-low thermal conductivity as well as elusive 'plasmonic salts'.

Data availability

All data supporting the findings of this study are available within this article and its ESI.† The X-ray crystallographic details for structures reported in this article have been deposited at the Cambridge Crystallographic Data Centre (CCDC), under deposition nos. CCDC2352448, CCDC2352449, and CCDC2352450 for (TMA)$AgBr_2$ at 150 K, 340 K and 298 K, respectively.

Author contributions

N. H. prepared the samples, carried out the experiments, and performed electrical transport measurements along with S. S. under the guidance of N. B.; S. N. performed DFT calculations under the supervision of K. T.; N. H. and S. S. wrote the first draft, which was finalized by N. B. with inputs from the co-authors; N. B. supervised the research project.

Conflicts of interest

The authors declare no competing financial interest.

Acknowledgements

N. B. acknowledges IISER Pune, India for financial support. K. T. acknowledges VGST (GRD No. 536) for financial support. K. T. and S. N. acknowledge C-DAC for providing the computational facility in PARAMUtkarsh. The support and the resources provided by "PARAM Brahma Facility" under the National Supercomputing Mission, Govt. of India at IISER Pune are gratefully acknowledged. N. H. and S. S. thank IISER Pune for providing Research Fellowships. N. H. acknowledges Mr Rishu Kumar Pandey for help in solving the crystal structure and Mr Ankit Kumar for help during thermal diffusivity measurements.

Notes and references

1 M. J. Katz, K. Sakai and D. B. Leznoff, The use of aurophilic and other metal–metal interactions as crystal engineering design elements to increase structural dimensionality, *Chem. Soc. Rev.*, 2008, **37**, 1884–1895.
2 S. Sculfort and P. Braunstein, Intramolecular d^{10}–d^{10} interactions in heterometallic clusters of the transition metals, *Chem. Soc. Rev.*, 2011, **40**, 2741–2760.
3 Q. Zheng, S. Borsley, G. S. Nichol, F. Duarte and S. L. Cockroft, The Energetic Significance of Metallophilic Interactions, *Angew. Chem., Int. Ed.*, 2019, **58**, 12617–12623.
4 A. Haque, K. M. Alenezi, M. S. Khan, W.-Y. Wong and P. R. Raithby, Non-covalent interactions (NCIs) in π-conjugated functional materials: advances and perspectives, *Chem. Soc. Rev.*, 2023, **52**, 454–472.
5 M. R. R. Prabhath, J. Romanova, R. J. Curry, S. R. P. Silva and P. D. Jarowski, The Role of Substituent Effects in Tuning Metallophilic Interactions and Emission Energy of Bis-4-(2-pyridyl)-1,2,3-triazolatoplatinum(II) Complexes, *Angew. Chem., Int. Ed.*, 2015, **54**, 7949–7953.
6 X.-Q. Zhou, M. Mytiliniou, J. Hilgendorf, Y. Zeng, P. Papadopoulou, Y. Shao, M. P. Dominguez, L. Zhang, M. B. S. Hesselberth, E. Bos, M. A. Siegler, F. Buda, A. M. Brouwer, A. Kros, R. I. Koning, D. Heinrich and S. Bonnet, Intracellular Dynamic Assembly of Deep-Red Emitting Supramolecular Nanostructures Based on the Pt…Pt Metallophilic Interaction, *Adv. Mater.*, 2021, **33**, 2008613.
7 X.-Q. Zhou, P. Wang, V. Ramu, L. Zhang, S. Jiang, X. Li, S. Abyar, P. Papadopoulou, Y. Shao, L. Bretin, M. A. Siegler, F. Buda, A. Kros, J. Fan, X. Peng, W. Sun and S. Bonnet, In vivo metallophilic self-assembly of a light-activated anticancer drug, *Nat. Chem.*, 2023, **15**, 980–987.
8 H. Schmidbaur and A. Schier, Aurophilic interactions as a subject of current research: an up-date, *Chem. Soc. Rev.*, 2012, **41**, 370–412.

9 N. Mirzadeh, S. H. Privér, A. J. Blake, H. Schmidbaur and S. K. Bhargava, Innovative Molecular Design Strategies in Materials Science Following the Aurophilicity Concept, *Chem. Rev.*, 2020, **120**, 7551–7591.
10 H. Schmidbaur and A. Schier, Argentophilic Interactions, *Angew. Chem., Int. Ed.*, 2015, **54**, 746–784.
11 Y.-Z. Huang, R. K. Gupta, G.-G. Luo, Q.-C. Zhang and D. Sun, Luminescence thermochromism in atomically precise silver clusters: a comprehensive review, *Coord. Chem. Rev.*, 2024, **499**, 215508.
12 N. V. S. Harisomayajula, S. Makovetskyi and Y.-C. Tsai, Cuprophilic Interactions in and between Molecular Entities, *Chem.–Eur. J.*, 2019, **25**, 8936–8954.
13 N. Hassan, S. Nagaraja, S. Saha, K. Tarafder and N. Ballav, Excitonic cuprophilic interactions in one-dimensional hybrid organic–inorganic crystals, *Chem. Sci.*, 2024, **15**, 4075–4085.
14 Z. Ma, X. Ji, S. Lin, X. Chen, D. Wu, X. Li, Y. Zhang, C. Shan, Z. Shi and X. Fang, Recent Advances and Opportunities of Eco-Friendly Ternary Copper Halides: A New Superstar in Optoelectronic Applications, *Adv. Mater.*, 2023, **35**, 2300731.
15 D. Banerjee and B. Saparov, Ultrabright Light Emission Properties of All-Inorganic and Hybrid Organic–Inorganic Copper(I) Halides, *Chem. Mater.*, 2023, **35**, 3364–3385.
16 L. Yao, K. Fu, X. Wang, M. He, W. Zhang, P.-Y. Liu, Y.-P. He and G. Liu, Metallophilic Interaction-Mediated Hierarchical Assembly and Temporal-Controlled Dynamic Chirality Inversion of Metal–Organic Supramolecular Polymers, *ACS Nano*, 2023, **17**, 2159–2169.
17 M.-M. Zhang, X.-Y. Dong, Z.-Y. Wang, X.-M. Luo, J.-H. Huang, S.-Q. Zang and T. C. W. Mak, Alkynyl-Stabilized Superatomic Silver Clusters Showing Circularly Polarized Luminescence, *J. Am. Chem. Soc.*, 2021, **143**, 6048–6053.
18 M. Cao, R. Pang, Q.-Y. Wang, Z. Han, Z.-Y. Wang, X.-Y. Dong, S.-F. Li, S.-Q. Zang and T. C. W. Mak, Porphyrinic Silver Cluster Assembled Material for Simultaneous Capture and Photocatalysis of Mustard-Gas Simulant, *J. Am. Chem. Soc.*, 2019, **141**, 14505–14509.
19 M. Zhao, S. Huang, Q. Fu, W. Li, R. Guo, Q. Yao, F. Wang, P. Cui, C.-H. Tung and D. Sun, Ambient Chemical Fixation of CO_2 Using a Robust Ag_{27} Cluster-Based Two-Dimensional Metal–Organic Framework, *Angew. Chem., Int. Ed.*, 2020, **59**, 20031–20036.
20 H. Wang, M. Wang, X. Xu, P. Gao, Z. Xu, Q. Zhang, H. Li, A. Yan, R. Y.-T. Kao and H. Sun, Multi-target mode of action of silver against Staphylococcus aureus endows it with capability to combat antibiotic resistance, *Nat. Commun.*, 2021, **12**, 3331.
21 M. Cao, S. Wang, J.-H. Hu, B.-H. Lu, Q.-Y. Wang and S.-Q. Zang, Silver Cluster-Porphyrin-Assembled Materials as Advanced Bioprotective Materials for Combating Superbacteria, *Adv. Sci.*, 2022, **9**, 2103721.
22 A. K. Das, S. Biswas, S. S. Manna, B. Pathak and S. Mandal, An atomically precise silver nanocluster for artificial light-harvesting system through supramolecular functionalization, *Chem. Sci.*, 2022, **13**, 8355–8364.
23 J. Kondo, Y. Tada, T. Dairaku, Y. Hattori, H. Saneyoshi, A. Ono and Y. Tanaka, A metallo-DNA nanowire with uninterrupted one-dimensional silver array, *Nat. Chem.*, 2017, **9**, 956–960.
24 R. Shannon, Revised effective ionic radii and systematic studies of interatomic distances in halides and chalcogenides, *Acta Crystallogr., Sect. A: Cryst. Phys., Diffr., Theor. Gen. Crystallogr.*, 1976, **32**, 751–767.
25 A. M. Ferraria, A. P. Carapeto and A. M. Botelho do Rego, X-ray photoelectron spectroscopy: silver salts revisited, *Vacuum*, 2012, **86**, 1988–1991.
26 J. F. Moulder, W. Stickle, P. Sobol and K. J. S. P. Bomben, *Handbook of X-ray photoelectron spectroscopy*, 1992.
27 P. Atkins, *Shriver and Atkins' inorganic chemistry*, Oxford University Press, USA, 2010.
28 H. W. T. Morgan, W. T. Laderer and A. N. Alexandrova, δ-Bonding and Spin-Orbit Coupling Make $SrAg_4Sb_2$ a Topological Insulator, *Chem.–Eur. J.*, 2024, **30**, e202303679.
29 C. Lepetit, P. Fau, K. Fajerwerg, M. L. Kahn and B. Silvi, Topological analysis of the metal-metal bond: a tutorial review, *Coord. Chem. Rev.*, 2017, **345**, 150–181.
30 C. Kittel, *Introduction to solid state physics*, 1986.
31 W. Lee, H. Li, A. B. Wong, D. Zhang, M. Lai, Y. Yu, Q. Kong, E. Lin, J. J. Urban, J. C. Grossman and P. Yang, Ultralow thermal conductivity in all-inorganic halide perovskites, *Proc. Natl. Acad. Sci. U. S. A.*, 2017, **114**, 8693–8697.
32 A. Das, K. Pal, P. Acharyya, S. Das, K. Maji and K. Biswas, Strong Antibonding I (p)–Cu (d) States Lead to Intrinsically Low Thermal Conductivity in $CuBiI_4$, *J. Am. Chem. Soc.*, 2023, **145**, 1349–1358.
33 M. Dutta, K. Pal, U. V. Waghmare and K. Biswas, Bonding heterogeneity and lone pair induced anharmonicity resulted in ultralow thermal conductivity and promising thermoelectric properties in n-type $AgPbBiSe_3$, *Chem. Sci.*, 2019, **10**, 4905–4913.
34 A. Mandal, S. Goswami, S. Das, D. Swain and K. Biswas, New Lead-free Hybrid Layered Double Perovskite Halides: Synthesis, Structural Transition and Ultralow Thermal Conductivity, *Angew. Chem., Int. Ed.*, 2024, e202406616.
35 H. Kobayashi, H. Cui and A. Kobayashi, Organic Metals and Superconductors Based on BETS (BETS = Bis(ethylenedithio)tetraselenafulvalene), *Chem. Rev.*, 2004, **104**, 5265–5288.
36 N. K. Tailor, C. A. Aranda, M. Saliba and S. Satapathi, Negative Photoconductivity: Bizarre Physics in Semiconductors, *ACS Mater. Lett.*, 2022, **4**, 2298–2320.
37 N. K. Tailor, P. Maity, M. I. Saidaminov, N. Pradhan and S. Satapathi, Dark Self-Healing-Mediated Negative Photoconductivity of a Lead-Free $Cs_3Bi_2Cl_9$ Perovskite Single Crystal, *J. Phys. Chem. Lett.*, 2021, **12**, 2286–2292.
38 N. K. Tailor, P. Maity and S. Satapathi, Observation of Negative Photoconductivity in Lead-Free $Cs_3Bi_2Br_9$ Perovskite Single Crystal, *ACS Photonics*, 2021, **8**, 2473–2480.
39 N. Krishnamurthy, Raman spectra of tetramethyl ammonium bromide and iodide, *Proc. Indian Acad. Sci.*, 1965, **61**, 164–171.